applied sciences

MDPI

Article

Radiomics Assessment of Iliac Bone Marrow on Prostate MRI Discriminates Monoclonal Gammopathy of Undetermined Significance with and Without Concomitant Prostate Cancer: A Proof-of-Concept Study

Giuseppe Salvaggio [1,*], Giuseppe Cutaia [1], Emanuele Gattuso [1], Elisabetta Raitano [1], Rossano Girometti [2], Silvia Sanità [2], Gabriele Tulone [3], Nicola Pavan [3], Anna Martorana [4], Cirino Botta [4] and Albert Comelli [5]

[1] Section of Radiology, Department of Biomedicine, Neuroscience and Advanced Diagnostics (BiND), University of Palermo, Via del Vespro 129, 90127 Palermo, Italy; giuseppe.cutaia@policlinico.pa.it (G.C.); emanuelegattuso96@gmail.com (E.G.); elisaraitano@gmail.com (E.R.)
[2] Institute of Radiology, Department of Medicine, University of Udine, University Hospital "S. Maria della Misericordia", Azienda Sanitaria Universitaria Friuli Centrale (ASUFC), 33100 Udine, Italy; rossanogirometti@uniud.it (R.G.); sanita.silvia@spes.uniud.it (S.S.)
[3] Department of Precision Medicine in the Medical, Surgical and Critical Care Area (Me.Pre.C.C.), University of Palermo, 90141 Palermo, Italy; gabriele.tulone@policlinico.pa.it (G.T.); nicola.pavan@unipa.it (N.P.)
[4] Department of Health Promotion, Mother and Child Care, Internal Medicine and Medical Specialties (ProMISE), University of Palermo, 90141 Palermo, Italy; anna.martorana@unipa.it (A.M.); cirino.botta@unipa.it (C.B.)
[5] Ri.MED Foundation, Via Bandiera 11, 90133 Palermo, Italy; acomelli@fondazionerimed.com
* Correspondence: giuseppe.salvaggio@policlinico.pa.it; Tel.: +39-0916552315

Abstract

Objectives: To investigate whether radiomics features extracted from iliac bone marrow on prostate MRI can differentiate patients with monoclonal gammopathy of undetermined significance (MGUS) alone from those with concomitant MGUS and prostate cancer (PCa). **Methods**: This retrospective study included 28 patients with hematologically confirmed MGUS who underwent multiparametric prostate MRI and MRI/ultrasound fusion-guided biopsy, stratified into MGUS + PCa (n = 16) and MGUS-only (n = 12). The right iliac bone marrow was manually segmented on axial T2-weighted images. A total of 107 radiomics features were extracted using PyRadiomics. A hybrid descriptive-inferential approach was applied for feature selection, followed by discriminant analysis with 5-fold cross-validation. Diagnostic performance was evaluated using sensitivity, specificity, accuracy, PPV, NPV, and AUROC with 95% bootstrap confidence intervals. **Results**: ANOVA identified two features with significant group differences. After hybrid feature selection, original_glcm_ClusterShade was the most discriminative feature. The model achieved sensitivity of 87.5%, specificity of 41.7%, accuracy of 67.9%, PPV of 66.7%, NPV of 71.4%, and AUROC of 0.745 (95% CI: 0.54–0.91; p = 0.013). **Conclusions**: Radiomics analysis of the iliac bone marrow on routine prostate MRI may reveal microstructural differences between patients with isolated MGUS and those with concomitant MGUS and PCa. These hypothesis-generating findings warrant prospective validation in larger multicenter cohorts before clinical application.

Keywords: radiomics; monoclonal gammopathy of undetermined significance; prostate neoplasm; bone marrow; magnetic resonance imaging; ilium

Academic Editors: Jia-Lien Hsu and Rui Araújo

Received: 16 May 2026
Revised: 1 July 2026
Accepted: 3 July 2026
Published: 7 July 2026

1. Introduction

Recent epidemiological studies have highlighted an emerging association between monoclonal gammopathy of undetermined significance (MGUS) and prostate cancer (PCa) [1–3]. Large population-based analyses have demonstrated that men with MGUS face a two-fold increased risk of developing PCa, with temporality analyses showing that MGUS commonly precedes the diagnosis [1]. This association appears independent of conventional risk factors such as age, body mass index, and family history, suggesting that shared lifestyle or genetic susceptibility alone does not fully explain the observed link [1].

Clinical case reports confirm the co-occurrence, whether synchronous or metachronous, of plasma cell dyscrasias and prostate cancer [2,4]. The biological interplay remains unclear; however, both conditions appear to share alterations in the bone marrow microenvironment and common pathogenic drivers such as cytokine signaling (IL-6, IGF-1, VEGF), immune suppression, and microenvironmental crosstalk [2,3].

Despite these observations, the pathophysiological mechanisms underpinning the MGUS–prostate cancer relationship remain elusive. Attention has increasingly shifted toward the bone marrow microenvironment as a possible site of convergence between these two conditions, where radiomics, through high-throughput quantitative analysis of medical images, offers a promising noninvasive tool to explore microstructural marrow changes.

To date, no study has leveraged bone marrow radiomics on prostate MRI to investigate this relationship. We hypothesize that patients with concomitant MGUS and PCa may exhibit distinctive radiomics signatures in the iliac bone marrow compared to those with MGUS alone, reflecting a shared disease-promoting microenvironment. Therefore, the primary objective of this proof-of-concept study is to determine whether radiomics features extracted from the iliac bone marrow on prostate MRI can differentiate patients with MGUS alone from those with concomitant MGUS and PCa. It should be noted that the computational methods employed (PyRadiomics feature extraction, ANOVA-based screening, and discriminant analysis with cross-validation) represent established radiomics tools; the genuine novelty resides in the clinical question itself. Rather than proposing a validated diagnostic solution, this study aims to provide a hypothesis-generating imaging framework based on clinically available data, potentially paving the way for novel noninvasive risk-stratification strategies.

2. Materials and Methods

2.1. Ethical Considerations and Informed Consent

This analysis was performed as part of the monocentric observational study 'MMVision,' approved by our institutional ethics committee (approval number 02/2022—15 February 2022) and conducted in accordance with the ethical standards of the Declaration of Helsinki. All patients provided written informed consent for the use of their anonymized imaging data for research purposes.

Artificial intelligence tools were used to assist in manuscript drafting and editing. All content was critically reviewed, verified, and approved by all authors.

2.2. Study Population and Design

The study population was derived from a prospectively maintained urology department database of 750 consecutive patients. Cross-referencing with hematology records identified 79 eligible patients with confirmed MGUS. Exclusion criteria were: (a) lack of multiparametric prostate MRI (n = 20); (b) lack of subsequent MRI-ultrasound fusion-guided biopsy with systematic random biopsy (n = 25); (c) isolated ASAP or high-grade PIN without concomitant adenocarcinoma (n = 6). MRI indications included prostatic symptoms, abnormal digital rectal examination, or elevated PSA (>2.5 ng/mL). All prostate

MRI examinations were interpreted using PI-RADS v2.1 before pathological results were available. Clinical data collected included age, BMI, smoking status, PSA, PSA ratio, PI-RADS score, serum free light chain kappa (FLCk) and lambda (FLCλ) concentrations, FLCk/FLCλ ratio, and biopsy results.

2.3. Hematological Diagnosis

The diagnosis of MGUS was established using standardized hematological assays including serum protein electrophoresis (SPE), serum immunosubtraction on capillary electrophoresis, immunofixation electrophoresis (IFE), and serum free light chain (FLC) assays. All patients diagnosed with MGUS were subsequently followed at the hematology outpatient clinic.

2.4. MRI Technique

MRI examinations were performed using a 3T MR scanner (Ingenia, Philips Healthcare, Best, The Netherlands) equipped with a 16-channel dStream Torso phased-array coil (Philips Healthcare, Best, The Netherlands); the same imaging protocol was used for all patients. No endorectal coil was used. Detailed pulse sequence parameters are reported in Table 1. In accordance with PI-RADS recommendations, all multiparametric prostate MRI examinations were performed at least 6 weeks after any prior prostate biopsy to allow complete reabsorption of post-procedural hemorrhagic foci.

Table 1. MRI imaging parameters for the study population at 3T MR system (Ingenia, Philips Healthcare, Best, The Netherlands).

Parameter	T1w TSE	T2w TSE	Diffusion-Weighted Imaging
TR (ms)	500–600	3500–4000	4000–6000
TE (ms)	10–15	90–110	60–80
Flip Angle (degrees)	90	90	90
Slice thickness (mm)	5	3	4
Reconstruction interval (mm)	0.5	0.3–0.5	0.4
Acquisition matrix	448 × 358	256 × 256	112 × 112
Signal averages (NSA)	1	2–3	6
Voxel size (mm)	0.78 × 1.12 × 5	0.6 × 0.6 × 3	3.0 × 3.0 × 4

TR = repetition time; TE = echo time; NSA = number of signal averages; TSE = turbo spin-echo; DWI = diffusion-weighted imaging.

The standard protocol included axial, coronal, and sagittal T2-weighted turbo spin-echo images of the prostate and seminal vesicles, axial T1-weighted turbo spin-echo images to detect post-biopsy blood residues, and diffusion-weighted imaging (b-values: 50, 800, and 1400 s/mm^2) with ADC maps. Following unenhanced imaging, patients received intravenous Gadoteric acid (Gd-DOTA, Dotarem, Guerbet, Villepinte, France) at 1 mmol/kg body weight and 3 mL/sec, followed by a 20–30 mL saline flush. Axial T1-weighted 3D spoiled gradient-recalled echo sequences were acquired after contrast to obtain dynamic contrast-enhanced (DCE) images.

Image quality was assessed using the PI-QUAL scoring system. All MRI studies had a PI-QUAL score of 3, ensuring diagnostic adequacy and minimizing radiomics feature distortion due to suboptimal acquisition. The main pulse sequence parameters are summarized in Table 1.

2.5. Manual Segmentation

Radiomics analysis was performed on axial T2-weighted images, which routinely include both iliac wings within the field of view. Although multiple osseous structures (such as the sacrum, lumbar spine, and femoral heads) were partially visible, segmentation was deliberately restricted to the right iliac wing. The selection of the right iliac wing was based on three convergent rationales: (1) the iliac crest is the standard site for bone marrow biopsy in hematological practice, conferring biological precedent for its relevance in MGUS assessment; (2) red (hematopoietic) marrow is most abundant in the iliac wings in adults, making this the most biologically relevant site for detecting plasma cell-related changes; (3) segmenting a single iliac wing ensures methodological consistency and eliminates laterality as a source of variability; the right side was selected by institutional convention.

Segmentation was manually performed by two radiologists with 15 and 5 years of experience in MRI interpretation, working independently and subsequently reaching consensus. Each MRI examination was imported into 3D Slicer (Boston, MA, USA) [5], an open-source platform widely used for medical image visualization and analysis. Using a closed polygon contouring tool, each radiologist traced the visible portion of the right iliac wing slice-by-slice on axial T2-weighted images, carefully excluding cortical bone and adjacent vascular structures. The segmented region was limited to the largest consistently visualized portion of the right iliac bone marrow, ensuring anatomical accuracy and reproducibility across patients (Figure 1).

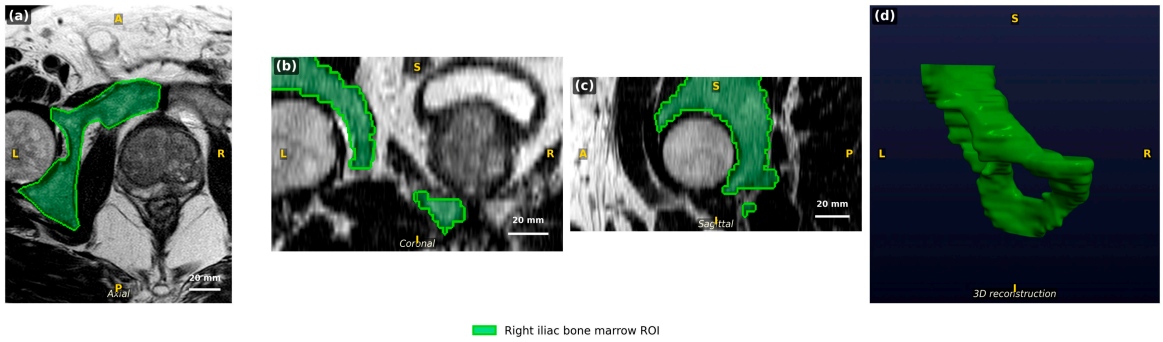

Figure 1. Manual segmentation of the right iliac bone marrow on multiparametric prostate MRI. Representative axial (**a**), coronal (**b**), and sagittal (**c**) views show the segmented region of interest (green overlay). Panel (**d**) shows the three-dimensional surface reconstruction of the segmentation volume. A = anterior; P = posterior; L = left; R = right; S = superior; I = inferior.

Inter-rater reliability was assessed by comparing the independent segmentations of the two radiologists. Feature-level reproducibility was evaluated using the intraclass correlation coefficient (ICC), yielding a mean ICC of 0.88 (two-way mixed effects model, single measures, absolute agreement), indicative of good-to-excellent inter-rater agreement. Geometric concordance between the two segmentation sets was quantified using the Dice similarity coefficient (DSC), with a mean DSC of 0.92 $\pm$ 0.03, confirming excellent spatial overlap.

2.6. Radiomics Feature Extraction and Imaging Analysis

From prostate MRI images, radiomics features were extracted using PyRadiomics (version 3.1.0) [6] from the iliac bone marrow. Extracted features encompassed shape, first-order statistical, and higher-order texture categories. Image normalization was applied using z-score normalization (Normalize = True, normalizeScale = 1) to reduce inter-patient signal variability inherent to T2-weighted acquisitions. Gray-level discretization was performed with a fixed bin width of 0.45 (BinWidth = 0.45), selected after preliminary evaluation to provide adequate texture sensitivity on normalized intensity distributions, consistent with

previously published bone marrow radiomics studies. No voxel resampling was applied; features were extracted at the native image resolution to preserve spatial information. The mask was interpolated using nearest-neighbor interpolation to avoid fractional label values. All remaining PyRadiomics settings were maintained at library defaults.

A one-way analysis of variance (ANOVA) was applied to all 107 extracted radiomics features to identify those with statistically significant differences between the two groups (MGUS + PCa and MGUS-only). Features with a p-value < 0.05 were retained for subsequent analysis. Among the ANOVA-selected features, an innovative sequential hybrid descriptive-inferential method was applied for feature selection and redundancy reduction. Specifically, for each selected feature, the point-biserial correlation coefficient was calculated between the feature values and the dichotomous outcome variable (MGUS + PCa = 1, MGUS-only = 0). Features were then ranked in descending order according to the absolute value of the point-biserial correlation coefficient. Subsequently, a stepwise cycle was initiated, adding one feature at a time and performing logistic regression analysis at each iteration. The p-value of each iteration was compared with that of the preceding iteration, and the cycle was stopped when the p-value no longer decreased. This procedure identified the most discriminative and non-redundant subset of radiomic features. Discriminant analysis was used to build a predictive model capable of distinguishing patients with isolated MGUS from those with concomitant MGUS and prostate cancer, using the features identified by the hybrid selection method. A 5-fold cross-validation strategy was used to divide the data into training and validation sets. At each iteration, one fold served as the validation set while the remaining folds constituted the training set, ensuring disjoint validation sets across all iterations. This process was repeated for each of the k = 5 folds. To quantify the magnitude of between-group differences for each radiomic feature, Cohen's d effect size was calculated for all 107 features, providing an interpretable measure of discriminative capacity independent of sample size.

2.7. Statistical Analysis

Diagnostic performance was assessed by sensitivity, specificity, accuracy, PPV, NPV, and AUROC with 95% bootstrap confidence intervals (2000 iterations). Statistical significance of the AUROC was assessed via permutation test (2000 permutations). Baseline characteristics were compared using the Mann–Whitney U test for continuous variables and Fisher's exact test for categorical variables (significance threshold: $p < 0.05$). All analyses were implemented in Python 3.12 (SciPy, scikit-learn, NumPy). No missing data were present in the radiomics feature dataset.

3. Results

3.1. Study Cohort Characteristics

Figure 2 portrays the subjects' accrual flowchart following the Strengthening the Reporting of Observational Studies in Epidemiology (STROBE) initiative (Supplementary Material S1).

After excluding 51 patients based on the predefined criteria, the final study cohort comprised 28 patients with MGUS [median age of 67 years (IQR 64–76)], who were stratified into two groups based on prostate biopsy results. Group 1 (MGUS + PCa), consisting of patients with concomitant MGUS and prostate adenocarcinoma, included 16 patients. Group 2 (MGUS-only), consisting of patients with MGUS and a negative prostate biopsy, included 12 patients. Baseline clinical and hematological characteristics of the two groups are summarized in Table 2.

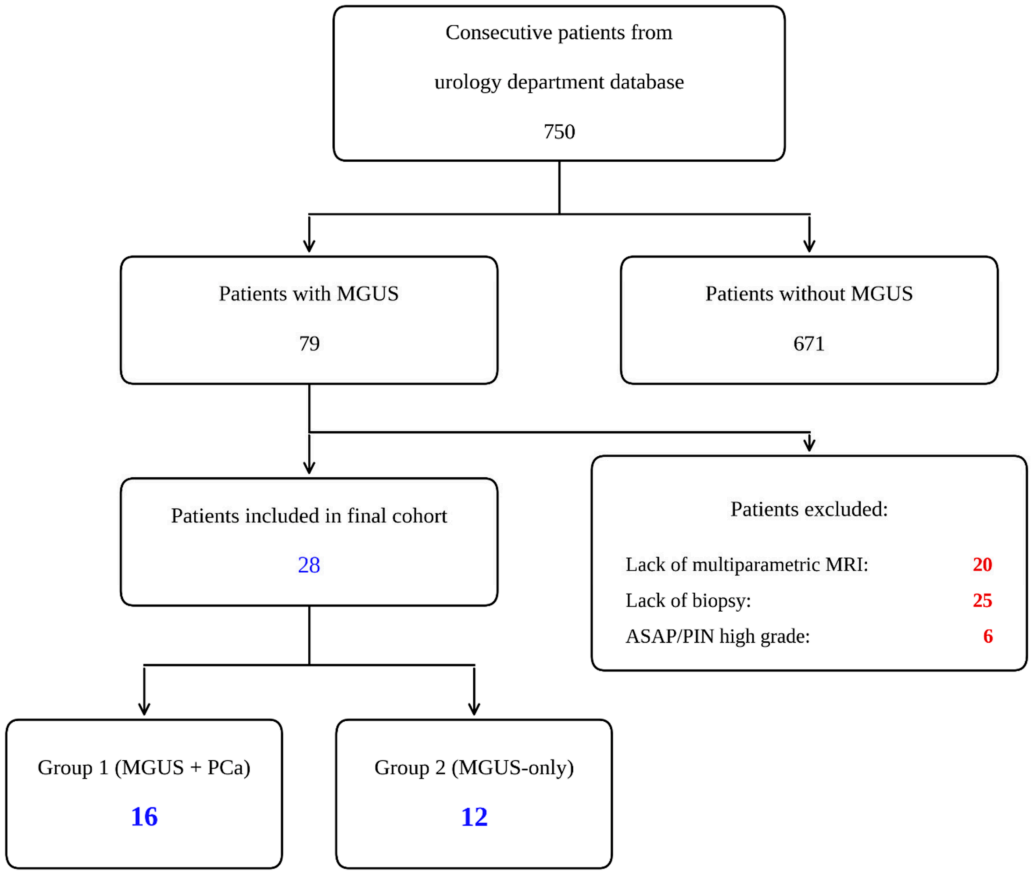

Figure 2. Flowchart illustrating subject accrual, exclusion criteria, and final stratification of the study cohort into MGUS + PCa and MGUS-only groups.

Table 2. Baseline clinical and hematological characteristics of the study cohort stratified by group.

Variable	MGUS + PCa (*n* = 16)	MGUS-Only (*n* = 12)	*p*-Value
Demographics			
Age, years—median (IQR)	72.0 (67.0–77.0)	65.0 (63.8–67.2)	0.071
BMI, kg/m^2—median (IQR)	25.7 (24.2–27.1)	26.4 (25.7–27.5)	0.367
Smoker, *n* (%)	4/16 (25%)	2/12 (17%)	0.673
Prostate-specific markers			
PSA, ng/mL—median (IQR)	7.6 (6.3–12.5)	5.0 (2.3–8.4)	0.109
PSA ratio, %—median (IQR)	15.0 (12.0–18.0)	17.0 (13.0–20.0)	0.606
PI-RADS 3, *n* (%)	2/16 (12%)	5/12 (42%)	—
PI-RADS 4, *n* (%)	10/16 (62%)	1/12 (8%)	—
PI-RADS 5, *n* (%)	3/16 (19%)	2/12 (17%)	—
No assignable PI-RADS lesion (IPB/prostatitis) *, *n* (%)	1/16 (6%)	4/12 (33%)	—
PI-RADS $\geq$ 4, *n* (%)	13/16 (81%)	3/12 (25%)	0.006
Hematological markers (MGUS)			
FLC kappa, mg/dL—median (IQR)	22.2 (21.0–25.2)	18.2 (15.9–28.8)	0.132
FLC lambda, mg/dL—median (IQR)	18.5 (16.7–23.1)	15.1 (13.1–19.6)	0.180
FLC ratio—median (IQR)	1.2 (1.0–1.4)	1.2 (1.2–1.3)	0.742

Data are expressed as median (interquartile range) for continuous variables, or as number and percentage for categorical variables. *p*-values calculated using Mann–Whitney U test for continuous variables and Fisher's exact test for categorical variables. For PI-RADS distribution rows, the overall comparison for PI-RADS $\geq$ 4 vs. <4 yielded $p = 0.006$. * No assignable PI-RADS lesion: cases in which MRI showed findings consistent with benign prostatic hyperplasia (BPH) or prostatitis only, without an identifiable target lesion warranting a PI-RADS score assignment. IQR = interquartile range; PSA = prostate-specific antigen; FLC = free light chain; PI-RADS = Prostate Imaging Reporting and Data System; BMI = body mass index.

No statistically significant differences were observed between groups in age, BMI, PSA levels, PSA ratio, FLC concentrations, FLC ratio, or smoking status (all $p > 0.05$), indicating that the two groups were well balanced with respect to demographic and hematological variables. The only significant difference between groups was the PI-RADS score distribution: PI-RADS ≥ 4 was observed in 13 of 16 MGUS + PCa patients (81%) compared with 3 of 12 MGUS-only patients (25%; $p = 0.006$), consistent with the higher prevalence of clinically significant MRI lesions in patients with confirmed prostate cancer.

Among the 16 patients in Group 1 (MGUS + PCa), the Gleason Score (GS) from targeted biopsy was distributed as: GS 6 (3 + 3) in 7 patients (43.8%), GS 7 (3 + 4) in 2 patients (12.5%), GS 7 (4 + 3) in 2 patients (12.5%), GS 8 (4 + 4) in 2 patients (12.5%), GS 9 (4 + 5) in 2 patients (12.5%), and GS 9 (5 + 4) in 1 patient (6.2%). This distribution indicates that the majority of detected prostate cancers (9 out of 16, 56.2%) were clinically significant (GS ≥ 7).

3.2. Hematological Characteristics

All 28 patients were diagnosed with MGUS. Isotype distribution was: IgGk ($n = 15$), IgGλ ($n = 7$), IgMk ($n = 1$), IgMλ ($n = 1$), light chain kappa ($n = 2$), and light chain lambda ($n = 2$). Per the Mayo Clinic risk stratification model, 25 patients were low risk and 3 low-intermediate risk for progression.

3.3. Radiomics Imaging Analysis Performance

One-way ANOVA identified 2 features with statistically significant differences between groups: original_glcm_ClusterShade ($p = 0.026$) and original_ngtdm_Contrast ($p = 0.041$) (Figures 3 and 4). Following hybrid feature selection, original_glcm_ClusterShade was identified as the most discriminative feature (point-biserial $|r| = 0.42$). The discriminant analysis model achieved an AUROC of 0.745 (95% bootstrap CI: 0.54–0.91; $p = 0.013$), sensitivity of 87.5%, specificity of 41.7%, accuracy of 67.9%, PPV of 66.7%, and NPV of 71.4% (Figure 5, Table 3). Cohen's d effect size analysis confirmed original_glcm_ClusterShade as the feature with the largest between-group difference (d = −0.90), followed by original_ngtdm_Contrast (d = 0.82), both representing large effect sizes. The negative sign of ClusterShade's d indicates that MGUS + PCa patients exhibited systematically lower values (mean −3.78) compared to MGUS-only patients (mean 0.22), consistent with the direction of discrimination identified by the hybrid selection procedure. These findings should be regarded as exploratory and hypothesis-generating, pending validation in larger cohorts.

Table 3. Performance metrics of the discriminant analysis model applied to the most discriminative iliac bone marrow radiomic feature (original_glcm_ClusterShade) using 5-fold cross-validation.

Metric	Value
AUROC (95% bootstrap CI)	0.745 (0.54–0.91)
Sensitivity	87.5%
Specificity	41.7%
Accuracy	67.9%
Positive Predictive Value (PPV)	66.7%
Negative Predictive Value (NPV)	71.4%
p-value	0.013

AUROC = area under the receiver operating characteristic curve; CI = confidence interval; PPV = positive predictive value; NPV = negative predictive value. *p*-value calculated using permutation test (2000 permutations).

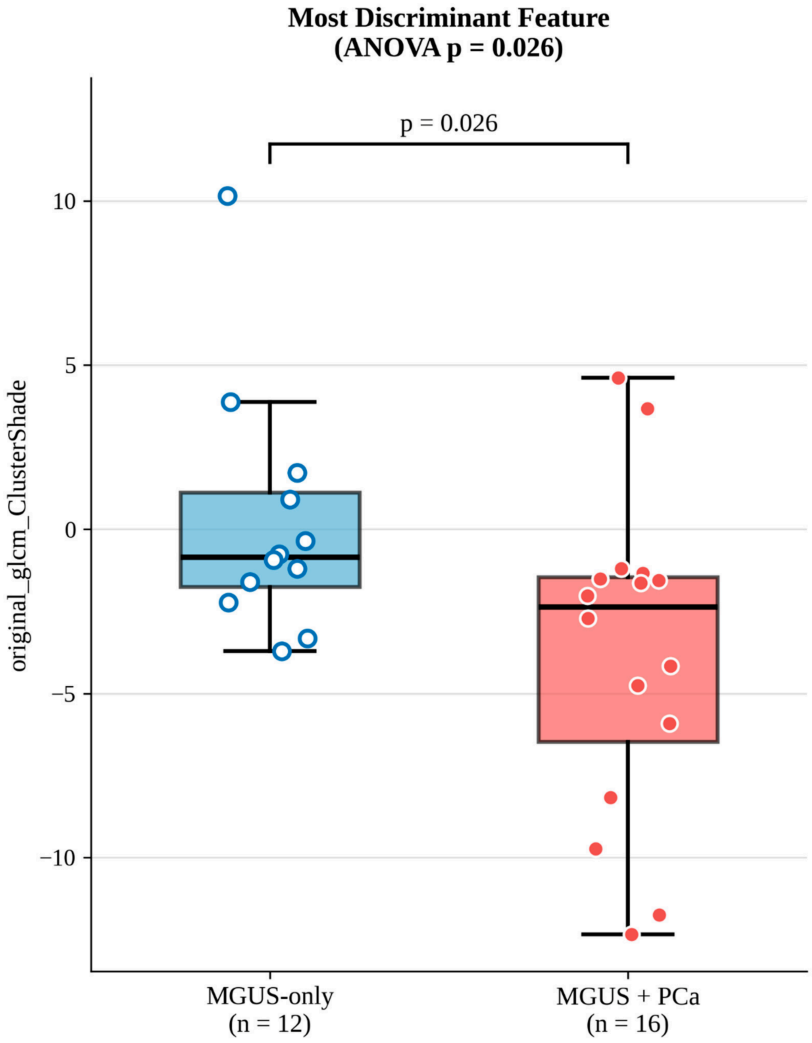

Figure 3. Box plot illustrating the distribution of the most discriminative radiomics feature (original_glcm_ClusterShade) identified by the hybrid descriptive-inferential selection method, showing group differences between MGUS-only (blue) and MGUS + PCa (red) patients (ANOVA $p = 0.026$). Individual data points are overlaid.

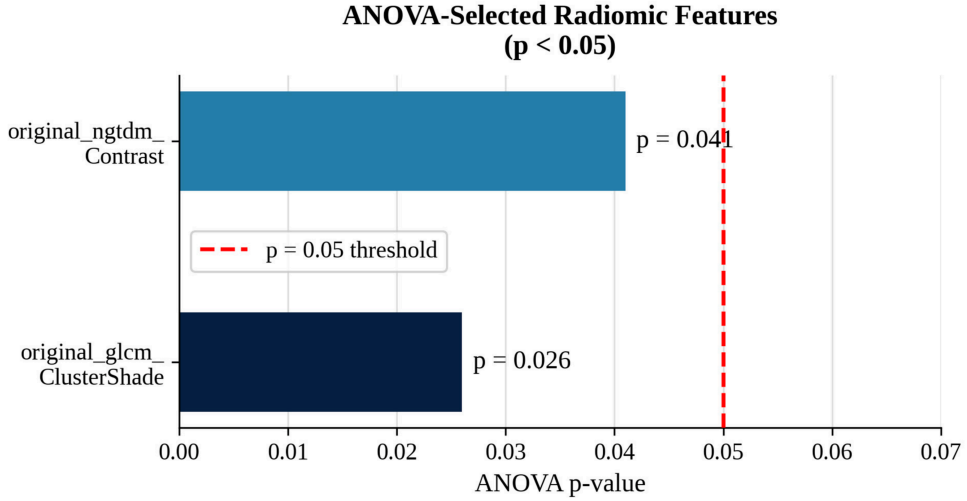

Figure 4. Bar plot illustrating the ANOVA *p*-values for the two radiomics features showing statistically significant group differences ($p < 0.05$) between MGUS-only and MGUS + PCa patients: original_glcm_ClusterShade ($p = 0.026$) and original_ngtdm_Contrast ($p = 0.041$).

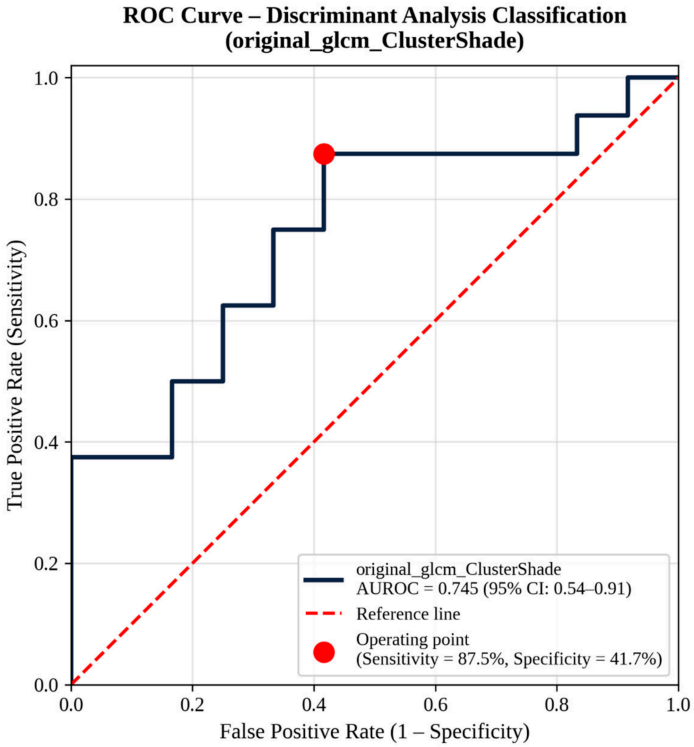

Figure 5. Receiver operating characteristic (ROC) curve for the discriminant analysis model applied to the most discriminative iliac bone marrow radiomics feature (original_glcm_ClusterShade) for the classification of MGUS-only versus MGUS + PCa patients. The area under the curve (AUROC) was 0.745 (95% bootstrap CI: 0.54–0.91; $p = 0.013$). The operating point corresponds to a sensitivity of 87.5% and a specificity of 41.7%.

3.4. Exploratory Cross-Institutional Application

The model was applied to three additional MGUS + PCa cases from an independent Academic Institution, using the same PyRadiomics configuration. Two cases (U02 and U03) were correctly classified as MGUS + PCa (discriminant scores: +1.53 and +1.29; predicted probabilities: 0.82 and 0.78). The third case (U01) was misclassified as MGUS-only (discriminant score: −0.91; predicted probability: 0.29); notably, its ClusterShade value (+4.12) fell outside the training group range (mean −3.78 ± 4.71), suggesting inter-institutional MRI variability or biological heterogeneity as possible contributors. These results are anecdotal and do not constitute formal external validation.

4. Discussion

This proof-of-concept study demonstrates, for the first time, that radiomics features extracted from the iliac bone marrow on prostate MRI can differentiate patients with MGUS alone from those with concomitant MGUS and prostate cancer, supporting the growing evidence of an association between monoclonal gammopathies and PCa [1–3]. Cytokines and growth factors such as IL-6, IGF-1, SDF-1, and VEGF have been implicated in the pathogenesis of both conditions, suggesting that a shared bone marrow microenvironment may represent the site of molecular cross-talk between plasma cell dyscrasias and prostate malignancy [2,3,7]. The biological rationale for expecting T2-weighted texture differences in iliac bone marrow of MGUS + PCa patients rests on three converging lines of evidence. First, bone marrow cytokine milieu is altered already at MGUS stage, not only in frank multiple myeloma. IL-6, a key mediator of bone marrow microenvironmental remodeling, has been shown to be increased in MGUS subjects [1,8]. IGF-1 has similarly been implicated as a potential accelerator of prostate cancer progression even at low-level plasma cell

infiltration [1]. This is a critical point: cytokine-driven marrow changes are not confined to frankly myelomatous marrow and may already be operative at the plasma cell infiltration levels characterizing MGUS (typically less than 10%). Second, monoclonal plasma cells and prostate cancer cells share a cytokine-enriched bone marrow microenvironment. IL-6, IGF-1, SDF-1, and VEGF—secreted by monoclonal plasma cells—not only support plasma cell survival but also promote progression toward clinically evident prostate cancer [2,9]. When prostate cancer coexists with MGUS, this shared cytokine milieu may further amplify marrow microenvironmental remodeling, producing a composite bone marrow phenotype distinguishable from MGUS alone. Third, a direct molecular link between monoclonal plasma cells and prostate cancer cells within the bone marrow niche has been identified through the GRP78/N-cadherin signaling axis [10]. GRP78, overexpressed in both myeloma and prostate cancer cells, promotes N-cadherin-mediated cell–cell interactions that sustain tumor survival and bone marrow colonization—providing mechanistic support for a composite marrow phenotype when both conditions coexist. At the MRI-texture level, these cumulative microenvironmental changes—including altered cellularity, extracellular matrix reorganization, and shifts in hematopoietic-to-fat marrow ratio—are expected to perturb the spatial co-occurrence patterns of T2 signal intensities that GLCM-derived features such as ClusterShade are specifically designed to capture. Our finding of lower ClusterShade values in MGUS + PCa patients (mean −3.78 vs. +0.22 in MGUS-only) is consistent with disruption of the asymmetric gray-level clustering patterns expected in more extensively remodeled marrow, though direct histopathological correlation was not available to confirm this interpretation. We acknowledge that the link between MGUS-level infiltration and detectable texture change remains inferential and requires prospective confirmation.

The model achieved an AUROC of 0.745 (95% bootstrap CI: 0.54–0.91), sensitivity of 87.5%, specificity of 41.7%, and accuracy of 67.9% (p = 0.013). The high sensitivity suggests a potential rule-out utility, whereby a negative model output could identify MGUS patients at low risk of concomitant PCa. However, the low specificity would result in a substantial false-positive rate, exposing patients to unnecessary biopsies. The NPV of 71.4% supports a potential role for this radiomics signature in identifying patients who could safely avoid immediate biopsy, though the moderate PPV (66.7%) cautions against relying on positive predictions without confirmatory biopsy. The wide confidence interval reflects statistical uncertainty inherent to the small sample size. Taken together, the limited sample size, low specificity, and absence of a validated external cohort indicate that this radiomics signature should not, at this stage, be interpreted as supporting immediate clinical applicability; these results should instead be regarded as a preliminary signal warranting prospective investigation.

The most discriminative feature, original_glcm_ClusterShade, is a GLCM-derived texture feature measuring the skewness and asymmetry of clusters of similar gray-level voxels. Its biological plausibility is supported by the bone marrow radiomics literature: Ekert et al. showed that MRI texture features from the iliac wing correlate with myeloma cell infiltration confirmed by biopsy (p = 0.006) [11]; Li et al. developed a radiomics nomogram predicting overall survival in multiple myeloma with a C-index of 0.812, outperforming established staging systems [12]; Bauer et al. demonstrated that pelvic bone marrow radiomics can predict therapy response in newly diagnosed myeloma across 8 centers (AUROC 0.70) [13]. At the microarchitectural level, monoclonal plasma cell infiltration is expected to disrupt the spatial organization of hematopoietic and fatty marrow, altering the co-occurrence patterns that ClusterShade captures; PCa-related microenvironmental remodeling may further amplify these changes. However, relying on a single feature introduces fragility, as GLCM features are sensitive to inter-institutional MRI protocol variability, as exemplified by the misclassified external case (U01). Future studies should

prioritize multivariate signatures and feature stability assessment across scanner vendors and protocols. Two methodological aspects warrant explicit discussion regarding the statistical reliability of the reported findings. First, ANOVA-based feature screening across 107 candidate features is inherently vulnerable to false-positive selection: at a threshold of $p < 0.05$, approximately five features are expected to reach significance by chance alone, and neither identified feature ($p = 0.026$ and $p = 0.041$) would survive Bonferroni (threshold $p < 0.00047$) or FDR correction. However, in the present pipeline ANOVA was employed not as a confirmatory hypothesis test but as a feature ranking and dimensionality reduction step within a machine learning framework—a role in which formal multiple comparison correction is not routinely required, as the aim is to identify candidate features for model training rather than to confirm inferential claims. Second, ANOVA screening was applied to the full dataset prior to cross-validation, so the validation folds were not fully independent from the feature selection step, introducing optimistic bias into the AUROC estimate. For these reasons, the reported AUROC of 0.745 should not be interpreted as a robust or generalizable benchmark: the wide bootstrap confidence interval (0.54–0.91) directly reflects this residual uncertainty. The identified features should be regarded as candidate signals and the overall results as hypothesis-generating, supporting the biological plausibility of bone marrow radiomics in this context and motivating prospective validation in larger cohorts.

The two groups were well balanced for all demographic and hematological variables (all $p > 0.05$), reducing the likelihood of confounding. Notably, PSA did not differ significantly between groups ($p = 0.109$), highlighting the limitations of this widely used marker in this specific clinical context and further supporting the rationale for complementary imaging-based approaches. Cohen's d effect size analysis further corroborated the discriminative relevance of ClusterShade ($d = -0.90$, large effect), confirming that the hybrid selection procedure identified the feature with the greatest between-group separation. The negative direction of the effect (MGUS + PCa patients exhibiting lower ClusterShade values) is consistent with microstructural marrow disruption reducing the asymmetry of gray-level cluster patterns captured by this feature. Critically, the radiomics model analyzes the iliac bone marrow rather than the prostate gland, making it conceptually and anatomically independent of the PI-RADS score and underscoring the novelty of the proposed approach. The exploratory application to three external cases, while yielding correct classification in two out of three instances, should be regarded as strictly hypothesis-generating. Future multicenter studies will be essential to establish clinical utility and to assess whether bilateral iliac segmentation, multivariate signatures, or complementary MRI sequences may improve discriminative performance. Should these findings be confirmed in larger prospective cohorts, any potential clinical utility would reside in a risk-enrichment role rather than in standalone classification: bone marrow radiomics could serve as a complementary screening signal to be integrated with established clinical and hematological variables, including PSA, FLC ratio, PI-RADS score, age, and MGUS risk stratification criteria, to identify MGUS patients at higher likelihood of harboring concomitant prostate cancer and to prioritize biopsy decisions accordingly. Future multicenter studies should systematically investigate whether combined radiomics-clinical signatures may improve discriminative performance and translational utility compared to single-feature radiomics alone. Several biological factors are known to influence bone marrow T2 signal intensity and texture independently of plasma cell infiltration, including anemia, osteoporosis, prior glucocorticoid or bisphosphonate use, and age-related fatty marrow conversion. These represent potential confounders of the radiomic signature identified in this study. Three considerations partially mitigate this concern: first, the two groups were balanced for age and BMI (all $p > 0.05$), reducing the likelihood that differential marrow aging or body composition contributed to the observed texture differences; second, patients with active

hematological conditions beyond confirmed MGUS were excluded by design; third, if residual confounders were randomly distributed across groups, their effect would introduce noise rather than systematic bias, tending to reduce rather than inflate the discriminative signal. Nonetheless, we cannot exclude that some contribution of ClusterShade values reflects non-disease-specific marrow changes. Future studies should prospectively collect and control for hemoglobin levels, DEXA scores, and medication history as covariates.

It should be noted that segmentation was restricted to the right iliac wing, and unilateral analysis may not capture bilateral or spatially heterogeneous marrow changes, a limitation that may be relevant in conditions with asymmetric marrow infiltration. Bilateral iliac segmentation, inclusion of sacral marrow, or whole-pelvis marrow analysis represent natural extensions of the present approach and should be systematically evaluated in future studies to determine whether broader anatomical coverage improves discriminative performance.

5. Limitations

A primary methodological limitation is the high risk of overfitting: with 107 radiomics features and only 28 patients, the feature-to-sample ratio is substantially unfavorable for robust model training. Although the hybrid feature selection reduced the feature space to a single variable prior to discriminant analysis, and 5-fold cross-validation was employed to mitigate this risk, the wide bootstrap CI of the AUROC (0.54–0.91) directly reflects the residual uncertainty. Model performance estimates should therefore be regarded as preliminary rather than validated benchmarks.

PPV and NPV are prevalence-dependent metrics; the values reported here reflect the specific PCa prevalence in our cohort (16/28, 57%) and would vary substantially in populations with different disease prevalence, warranting caution when extrapolating to other clinical settings.

A further limitation is potential selection bias: all patients underwent prostate MRI and biopsy due to clinical suspicion of PCa, meaning the MGUS-only group represents a specific subset with features mimicking prostate cancer rather than the general MGUS population. Whether findings apply to asymptomatic MGUS patients without prostate-related concerns remains unknown.

The small sample size, retrospective single-center design, and lack of a formal external validation cohort further limit generalizability, though these reflect the rare and underinvestigated nature of the MGUS-PCa association.

Reference standard bias should also be acknowledged, as radical prostatectomy is the only definitive method to rule out clinically significant PCa; however, all patients with negative biopsies underwent both fusion-targeted and systematic random biopsies, minimizing the likelihood of missing occult cancer [14,15].

Model calibration was not formally assessed. Given the small sample size (n = 28), calibration metrics (e.g., Hosmer–Lemeshow goodness-of-fit test) and calibration plots would be statistically underpowered and potentially misleading in the current cohort. Calibration analysis should be incorporated in future, adequately powered, validation studies. Formal adherence to TRIPOD + AI reporting guidelines was not feasible given the inherent constraints of this exploratory work.

Only inter-observer reproducibility of segmentation was assessed in this study; intra-observer agreement was not evaluated and should be incorporated in future validation studies.

Finally, radiomics extraction was restricted to axial T2-weighted images, as DWI sequences were considered less suitable due to lower spatial resolution and frequent artifacts affecting non-prostatic tissues.

6. Conclusions

This proof-of-concept study provides preliminary evidence that radiomics analysis of the iliac bone marrow on routine prostate MRI may capture a distinctive imaging phenotype associated with concomitant MGUS and prostate cancer, reflecting microstructural differences in the shared bone marrow microenvironment. A single texture feature (original_glcm_ClusterShade) demonstrated a potential discriminatory signal (AUROC 0.745), though the low specificity (41.7%) and wide confidence interval (0.54–0.91) underscore the substantial uncertainty of these estimates. The exploratory application to three external cases, with one misclassification, further highlights the fragility of single-feature models and the challenges of cross-institutional generalizability.

These findings should be regarded strictly as hypothesis-generating and must not guide clinical decisions at this stage, but reinforce the biological plausibility of a shared bone marrow microenvironmental signature in patients with dual pathology. Prospective validation in adequately powered, multicenter cohorts with standardized imaging protocols is an essential prerequisite before any consideration of radiomics as a tool for non-invasive risk stratification in MGUS patients.

Supplementary Materials: The following supporting information can be downloaded at: https://www.mdpi.com/article/10.3390/app16136814/s1, Supplementary Material S1: STROBE Statement—Checklist of items that should be included in reports of cohort studies.

Author Contributions: Conceptualization, G.S.; Methodology, G.S., A.M. and A.C.; Software, A.C.; Validation, G.S., G.C. and A.C.; Formal Analysis, G.S. and A.C.; Investigation, G.S., E.G., E.R., R.G., S.S., G.T., N.P. and C.B.; Resources, G.C. and E.G.; Data Curation, A.C.; Writing—Original Draft Preparation, G.S. and A.C.; Writing—Review and Editing, G.S. and A.C.; Visualization, G.S.; Project Administration, G.S. All authors have read and agreed to the published version of the manuscript.

Funding: This research received no external funding.

Institutional Review Board Statement: The study was conducted in accordance with the Declaration of Helsinki, and approved by the Institutional Ethics Committee of the University of Palermo (protocol code 02/2022; date of approval 15 February 2022).

Informed Consent Statement: Informed consent was obtained from all subjects involved in the study.

Data Availability Statement: The data presented in this study are available on request from the corresponding author due to privacy restrictions.

Acknowledgments: During the preparation of this manuscript, the authors used Claude 3.5 Sonnet (Anthropic, San Francisco, CA, USA; claude.ai) for the purposes of manuscript drafting and editing. The authors have reviewed and edited the output and take full responsibility for the content of this publication.

Conflicts of Interest: The authors declare no conflicts of interest.

References

1. Hornung, N.; Frank, M.; Dragano, N.; Dürig, J.; Dührsen, U.; Moebus, S.; Erbel, R.; Stang, A.; Jöckel, K.-H.; Schmidt, B. Monoclonal Gammopathy of Undetermined Significance Is Associated with Prostate Cancer in a Population-Based Cohort Study. *Sci. Rep.* **2021**, *11*, 19266. [CrossRef]
2. Pokhrel, A.; Heravi, O.; Enayati, L.; Nelson, R.; Mooppan, U.; Wu, R.; Wang, J.C. Association between Prostate Carcinoma and Multiple Myeloma. *Discov. Med.* **2023**, *35*, 664–672. [CrossRef]
3. Pramanik, S.; Gazi, M.J.; Das, A.K.; Debnath, N.B.; Pal, S.K. Monoclonal Gammopathy in Prostate Carcinoma: A Case Report and Review of Literature. *J. Med. Case Rep.* **2018**, *12*, 325. [CrossRef] [PubMed]
4. Allahyari, A.; Maharati, A.; Jafari-Nozad, A.M.; Zangooie, A. Prostate Cancer, Chronic Myelogenous Leukemia and Multiple Myeloma in a Single Patient: A Case Report and Review of the Literature. *J. Med. Case Rep.* **2023**, *17*, 35. [CrossRef] [PubMed]

5. Fedorov, A.; Beichel, R.; Kalpathy-Cramer, J.; Finet, J.; Fillion-Robin, J.-C.; Pujol, S.; Bauer, C.; Jennings, D.; Fennessy, F.; Sonka, M.; et al. 3D Slicer as an Image Computing Platform for the Quantitative Imaging Network. *Magn. Reson. Imaging* **2012**, *30*, 1323–1341. [CrossRef] [PubMed]
6. Van Griethuysen, J.J.M.; Fedorov, A.; Parmar, C.; Hosny, A.; Aucoin, N.; Narayan, V.; Beets-Tan, R.G.H.; Fillion-Robin, J.-C.; Pieper, S.; Aerts, H.J.W.L. Computational Radiomics System to Decode the Radiographic Phenotype. *Cancer Res.* **2017**, *77*, e104–e107. [CrossRef] [PubMed]
7. Kumar Upadhyay, A.; Kumar, M.; Kumar, A.; Prasad, A.; Prakash, A. Association Between Synchronous Occurrence of Multiple Myeloma and Carcinoma Prostate: Literature Analysis in the Context of a Case Report. *Cureus* **2023**, *15*, e48523. [CrossRef] [PubMed]
8. Allegra, A.; Innao, V.; Allegra, A.G.; Pugliese, M.; Di Salvo, E.; Ventura-Spagnolo, E.; Musolino, C.; Gangemi, S. Lymphocyte Subsets and Inflammatory Cytokines of Monoclonal Gammopathy of Undetermined Significance and Multiple Myeloma. *Int. J. Mol. Sci.* **2019**, *20*, 2822. [CrossRef] [PubMed]
9. Kao, J.; Jani, A.B.; Vijayakumar, S. Is There an Association between Multiple Myeloma and Prostate Cancer? *Med. Hypotheses* **2004**, *63*, 226–231. [CrossRef] [PubMed]
10. Cultrara, C.N.; Kozuch, S.D.; Ramasundaram, P.; Heller, C.J.; Shah, S.; Beck, A.E.; Sabatino, D.; Zilberberg, J. GRP78 Modulates Cell Adhesion Markers in Prostate Cancer and Multiple Myeloma Cell Lines. *BMC Cancer* **2018**, *18*, 1263. [CrossRef] [PubMed]
11. Ekert, K.; Hinterleitner, C.; Baumgartner, K.; Fritz, J.; Horger, M. Extended Texture Analysis of Non-Enhanced Whole-Body MRI Image Data for Response Assessment in Multiple Myeloma Patients Undergoing Systemic Therapy. *Cancers* **2020**, *12*, 761. [CrossRef] [PubMed]
12. Li, Y.; Liu, Y.; Yin, P.; Hao, C.; Sun, C.; Chen, L.; Wang, S.; Hong, N. MRI-Based Bone Marrow Radiomics Nomogram for Prediction of Overall Survival in Patients with Multiple Myeloma. *Front. Oncol.* **2021**, *11*, 709813. [CrossRef] [PubMed]
13. Bauer, F.; Hajiyianni, M.; Weinhold, N.; Grözinger, M.; Kächele, J.; Menis, E.; Raab, M.-S.; Sauer, S.; Jauch, A.; Weber, T.F.; et al. Automated Radiomics Model for Prediction of Therapy Response and Minimal Residual Disease from Baseline MRI in Multiple Myeloma. *Sci. Rep.* **2025**, *15*, 35400. [CrossRef] [PubMed]
14. in de Braekt, T.; van Rooij, S.B.T.; Daniels-Gooszen, A.W.; Scheepens, W.A.; de Jongh, R.; Bosch, S.L.; Nederend, J. Accuracy of MRI-Ultrasound Fusion-Guided and Systematic Biopsy of the Prostate. *Br. J. Radiol.* **2024**, *97*, 1132–1138. [CrossRef] [PubMed]
15. Liu, W.; Kadier, A.; Shen, D.; He, Y.; Dong, S.; Zhu, K.; Xu, G.; Zhao, B.; Mao, S.; Guo, C.; et al. Combined MRI-TRUS Fusion Targeted and Systematic Biopsy versus Systematic Biopsy Alone for the Detection of Prostate Cancer: Protocol for a Prospective Single-Centre Trial. *BMJ Open* **2024**, *14*, e080593. [CrossRef] [PubMed]